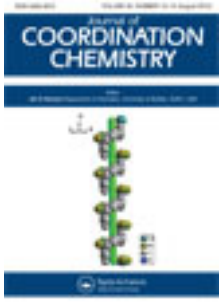

Journal of Coordination Chemistry
Publication details, including instructions for authors and subscription information:
http://www.tandfonline.com/loi/gcoo20

Phase transitions and molecular reorientations in $[Mn(OS(CH_3)_2)_6](ClO_4)_2$ studied by proton magnetic resonance and Raman spectroscopy

Elżbieta Szostak [a], Anna Migdał-Mikuli [a], Krystyna Hołderna-Natkaniec [b], Roman Gwoździk-Bujakowski [b] & Agnieszka Kaczor [a]

[a] Faculty of Chemistry, Department of Chemical Physics, Jagiellonian University, No. 3 Ingardena Street, 30-060 Kraków, Poland

[b] Institute of Physics, A. Mickiewicz University, No. 85 Umultowska Street, 61-606 Poznań, Poland

Accepted author version posted online: 11 Jun 2012.Published online: 22 Jun 2012.

To cite this article: Elżbieta Szostak, Anna Migdał-Mikuli, Krystyna Hołderna-Natkaniec, Roman Gwoździk-Bujakowski & Agnieszka Kaczor (2012) Phase transitions and molecular reorientations in $[Mn(OS(CH_3)_2)_6](ClO_4)_2$ studied by proton magnetic resonance and Raman spectroscopy, Journal of Coordination Chemistry, 65:15, 2732-2742, DOI: 10.1080/00958972.2012.702270

To link to this article: http://dx.doi.org/10.1080/00958972.2012.702270

Journal of Coordination Chemistry
Vol. 65, No. 15, 10 August 2012, 2732–2742

Phase transitions and molecular reorientations in $[Mn(OS(CH_3)_2)_6](ClO_4)_2$ studied by proton magnetic resonance and Raman spectroscopy

ELŻBIETA SZOSTAK*†, ANNA MIGDAŁ-MIKULI†, KRYSTYNA HOŁDERNA-NATKANIEC‡, ROMAN GWOŹDZIK-BUJAKOWSKI‡ and AGNIESZKA KACZOR†

†Faculty of Chemistry, Department of Chemical Physics, Jagiellonian University, No. 3 Ingardena Street, 30-060 Kraków, Poland
‡Institute of Physics, A. Mickiewicz University, No. 85 Umultowska Street, 61-606 Poznań, Poland

(*Received 28 December 2011; in final form 14 May 2012*)

The temperature dependence of full width at half maximum of bands associated with $\delta_d(OClO)F_2$, $\delta(CSC)$, and $\rho(CH_3)$ vibrational modes in the FT-RS spectra of $[Mn(OS(CH_3)_2)_6](ClO_4)_2$ have shown that the dynamic of reorientational motions of ClO_4^- and CH_3 groups (from $(CH_3)_2SO$) undergoes distinct changes at the phase transitions at $T^h_{C3} \approx 365\,K$ and $T^h_{C4} \approx 322\,K$. These are the phase transitions from stable crystal to stable rotational phase and from metastable crystal to metastable rotational phase, respectively. Moreover, characteristic changes of the Raman spectra at these phase transitions, connected with both the shift of the band positions and the scattered light intensity of the bands associated with $\nu_s(SO)$, $\nu_s(MnO)$, $\delta(CSC)$, and $\delta(OMnO)$ modes, suggest that these phase transitions are associated with crystal structure changes, too. Analysis of temperature dependence of the second moment (M_2) of ^1H NMR showed that on first heating (from room temperature) of the compound the reorientations of the CH_3 groups were set in motion in the phase transition at $T^h_{C3} \approx 365\,K$. On subsequent heating (after cooling the compound to 100 K) molecular reorientation starts just above 150 K, and above the temperature of 223 K all molecular groups containing protons perform nearly free rotation with frequencies of a few kHz, including an isotropic reorientation of the whole $[Mn(OS(CH_3)_2)_6]^{2+}$.

Keywords: Hexadimethylsulphoxidemanganese(II) chlorate(VII); Phase transition; Reorientational molecular motions; FT-RS; ^1H NMR

1. Introduction

Our recent investigations of $[M(OS(CH_3)_2)_6](ClO_4)_2$, where $M^{2+} = Mn^{2+}$, Cd^{2+}, Co^{2+}, and Zn^{2+}, show at least three different stable or metastable solid phases [1–4]. Some of these phases can be assigned to the plastic crystals called also orientational disordered crystals [5, 6]. In the plastic phase, the material flows readily under relatively low forces and can deform without fracture under stress [7, 8]. Plastic crystals are formed mainly

*Corresponding author. Email: szostak@chemia.uj.edu.pl

ISSN 0095-8972 print/ISSN 1029-0389 online
http://dx.doi.org/10.1080/00958972.2012.702270

by quasi-spherical or disk-like molecules [9]. The formation of plastic phase is related to releasing the rotational degrees of freedom of molecular groups occurring in the coordination compound. Such transition is usually associated with large enthalpy and entropy increases and can be observed by the DSC method. Orientationally disordered plastic crystals after quenching can form solids with frozen molecular orientations. The state is glasslike and the solids are sometimes called glassy-crystals [10, 11]. Plastic crystals are very interesting materials because they find applications as a new type of electrolyte for high energy density electrochemical devices such as lithium batteries and fuel cells [7, 12–16].

DSC measurements performed for $[Mn(OS(CH_3)_2)_6](ClO_4)_2$ from 170–400 K indicated evidence of four phase transitions above room temperature (RT), namely at $T^h_{C4} \approx 322$ K, $T^h_{C3} \approx 365$ K, $T^h_{C2} \approx 376$ K, $T^h_{C1} \approx 379$ K [1] and only one phase transition below RT at *ca* $T^h_{C5} \approx 223$ K [2]. $[Mn(OS(CH_3)_2)_6](ClO_4)_2$ crystallizes at RT in orthorhombic system, space group Fdd2, No 43, prototype GeS_2 (C44) structure, point group mm2 (C_{2v}), with lattice parameters, $a = 25.4425(6)$ Å, $b = 12.4043(3)$ Å, $c = 20.1696(5)$ Å, $V = 6365.2(3)$ Å^3, $Z = 8$ [17]. The crystal structure of this compound comprises discrete $[Mn(DMSO)_6]^{2+}$ (DMSO = $(CH_3)_2SO$) and ClO_4^- ions, all of which lie on crystallographic twofold axes. The oxygen atoms of six DMSO molecules are bonded to Mn^{2+} in a distorted octahedral geometry.

The aim of this study was to find connections between the phase transitions in $[Mn(OS(CH_3)_2)_6](ClO_4)_2$ and changes of the crystal structure and/or of the reorientational dynamic motions of $-CH_3$ in $(CH_3)_2SO$ (DMSO) ligands and ClO_4^-.

2. Experimental procedure

Synthesis of the title compound was described in our previous paper [1]. The results of chemical and thermal analysis of this compound confirmed its composition as $[Mn(OS(CH_3)_2)_6](ClO_4)_2$ as well as high chemical purity of the sample [1]. The band positions determined from FT-IR and FT-RS spectra at RT, proposed band assignments and comparison with the literature data [17–19] were collected in our previous paper [2].

Raman light scattering spectra (FT-RS) were recorded on a MultiRAM FT-Raman spectrometer equipped with a 1064-nm laser line (Nd:YAG laser power set on 250 mW) and with a germanium detector. All spectra were collected in a 4000–50 cm^{-1} range with 4 cm^{-1} resolution, and a total of 64 scans were accumulated. A Linkam THMS600 heating and freezing stage was used to take measurements in the temperature range 260–393 K with heating and cooling rate of 10 K min^{-1}.

The first derivative of absorption ^{1}H NMR signal from the radio frequencies field was recorded on a laboratory made instrument operating in the double modulation system, by the linear change in frequency of the autodyne generator from 25.375 to 25.625 MHz (i.e., first modulation is 250 KHz), at a constant magnetic field of 0.6 T. The signal was averaged and corrected for the amplitude of second modulation. The measurements were performed in two parts, first on heating the sample from 290 up to 390 K and the second on heating it from 100 to 400 K.

3. Results and discussion

In our previous paper [1] using DSC method, we discovered six phase transitions for $[Mn(OS(CH_3)_2)_6](ClO_4)_2$ in the temperature range 170–480 K and melting point at 487.6 K. On heating the compound possesses four stable solid phases. Two (Cr 1 and Cr 2) are more or less ordered and the next two (Rot 1 and Rot 2) are orientationally disordered phases, so-called rotational phases or plastic crystals. However, on cooling the compound possesses only three solid phases, which all have metastable character, one which is ordered (Cr 3) and two which are rotational phases (supercooled Rot 1 and Rot 3). All these phases can be presented in the form of temperature dependence of free enthalpy G as a schematic diagram, as shown in figure 1. The temperatures, enthalpy, and entropy changes of these phase transitions are presented in table 1.

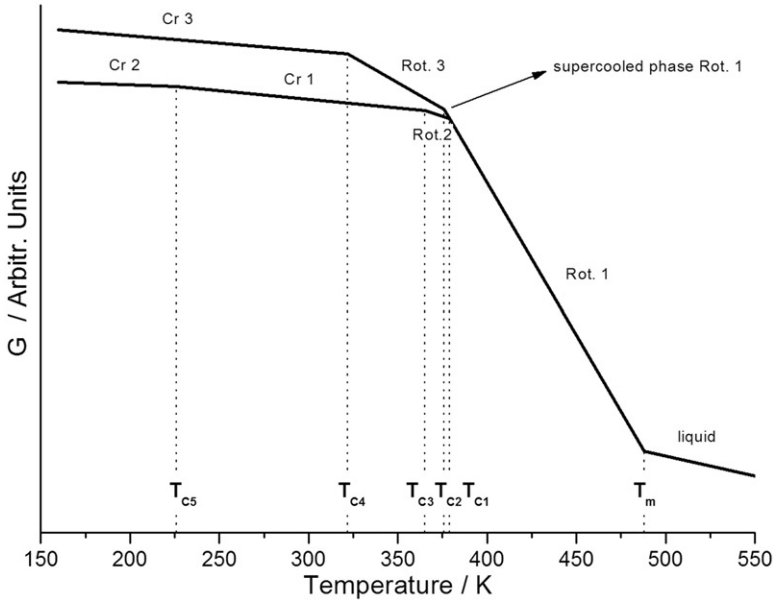

Figure 1. Schematic diagram of temperature dependence of the free enthalpy (G) of $[Mn(DMSO)_6](ClO_4)_2$.

Table 1. Thermodynamic parameters of the detected phase transitions on heating (T^h_{Cn}) and cooling (T^c_{Cn}) of $[Mn(DMSO)_6](ClO_4)_2$.

$[Mn(DMSO)_6](ClO_4)_2$						
Heating				Cooling		
T_{cn} (K)	$\overline{\Delta T} \pm S_{\Delta T}$ (K)	$\overline{\Delta H} \pm S_{\Delta H}$ (kJ mol^{-1})	$\overline{\Delta S} \pm S_{\Delta S}$ (J mol^{-1} K^{-1})	$\overline{\Delta T} \pm S_{\Delta T}$ (K)	$\overline{\Delta H} \pm S_{\Delta H}$ (kJ mol^{-1})	$\overline{\Delta S} \pm S_{\Delta S}$ (J mol^{-1} K^{-1})
T_{C1}	378.7 ± 1.1	3.43 ± 0.40	9.07 ± 1.06	–	–	–
T_{C2}	375.7 ± 2.2	4.44 ± 0.45	11.83 ± 1.21	370.2 ± 2.3	5.27 ± 0.45	14.24 ± 1.19
T_{C3}	364.7 ± 3.0	27.11 ± 1.24	74.33 ± 2.86	–	–	–
T_{C4}	321.6 ± 2.5	16.60 ± 0.62	51.63 ± 1.82	315.4 ± 3.5	16.39 ± 0.76	51.96 ± 2.33
T_{C5}	225.4 ± 0.1	0.88 ± 0.11	1.99 ± 0.25	222.9 ± 0.2	0.84 ± 0.21	1.87 ± 0.47

3.1. *FT-RS investigations*

The vibrations of $[Mn(OS(CH_3)_2)_6]^{2+}$ can be resolved into 177 normal modes, including 138 modes belonging to the 12 methyls. According to group theory, the vibrational representation of $[Mn(DMSO)_6]^{2+}$ under S_6 point group is $\Gamma_{vib} = 29A_g + 29E_g + 30A_u + 30E_u$. All gerade modes (g) should be Raman-active whereas the ungerade ones (u) should be IR-active [18]. The possible symmetry lowering in the solid state, from S_6 at least to C_3, can cause all vibrations to be both infrared- and Raman-active. However, the complementary character of the presented spectra and the very good agreement between theory and experiment shows that the geometry of $[Mn(DMSO)_6]^{2+}$ can be successfully described within S_6 symmetry, indicating lack of significant geometric distortion.

The ClO_4^- has nine normal modes. The vibrational representation of ClO_4^- under T_d point group is $\Gamma_{vib} = A_1 + E + 2F_2$. Thus, an isolated ClO_4^- has four vibration frequencies (in wavenumbers), $\nu_1 = \nu_s(ClO)A_1 = 928\,cm^{-1}$, $\nu_2 = \delta_d(OClO)E = 459\,cm^{-1}$, $\nu_3 = \nu_{as}(ClO)F_2 = 1119\,cm^{-1}$, and $\nu_4 = \delta_d(OClO)F_2 = 625\,cm^{-1}$, and all of them are Raman active [19–21]. In ionic crystal lattices, most of the vibrations contain contributions from many other internal coordinates and involve the motion of a relatively large number of atoms; however, the obtained spectra can be clearly divided into a few wavenumber ranges, connected with the sets of characteristic vibrations.

The FT-RS spectra of $[Mn(DMSO)_6](ClO_4)_2$ within the wavenumber range 4000–$50\,cm^{-1}$ were registered during heating, cooling, and subsequent heating of the sample in the temperature range 263–393 K. Figure 2 presents thermal evolutions of the FT-RS spectra recorded during first heating of the sample from 273–392 K in the wavenumber range in which the most significant changes occur. Significant differences between the

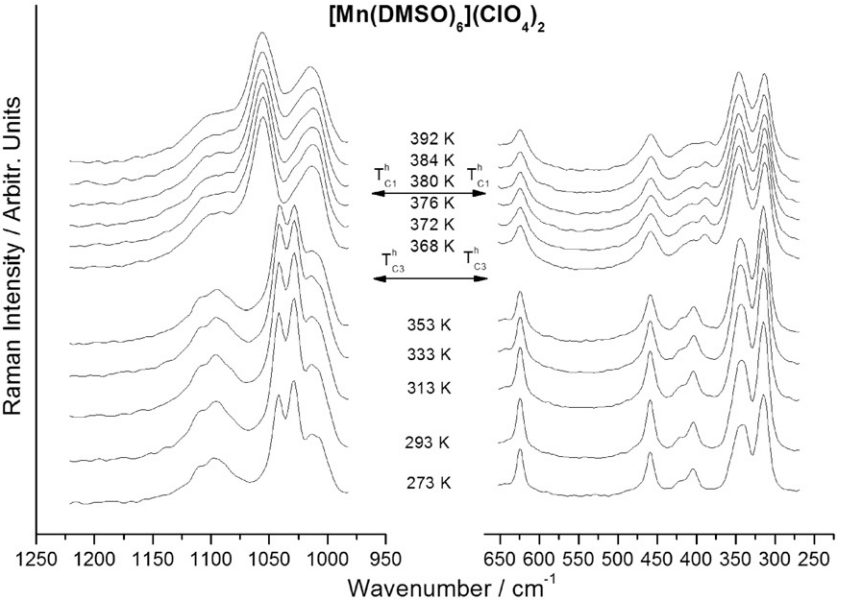

Figure 2. Temperature evolution of the FT-RS spectra of $[Mn(DMSO)_6](ClO_4)_2$. Horizontal arrows indicate temperature of the phase transitions registered by DSC [1] at heating.

spectra obtained below and above the phase transition at $T_{C3}^{h} \approx 365\,\mathrm{K}$ can be noticed. Above the phase transition temperature T_{C3}^{h} (figure 2), a distinct shift of the bands at 1041 and 1028 cm^{-1} (both associated with ν_s(SO) modes) toward higher and lower wavenumbers, respectively, could be observed. Beside a systematic decrease of intensity of the bands at 625 and 460 cm^{-1}, also decrease of the intensity and shift toward lower wavenumber of the band at 403 cm^{-1} (ν_s(MnO) mode) and characteristic changes in the relative intensity (inversion) of the bands at *ca* 314 and 344 cm^{-1}, associated with δ(CSC) and δ(OMnO) modes, respectively, can be clearly seen.

In order to verify whether the high temperature phase transitions registered during first heating of the sample are connected with a change in the reorientational dynamics of ClO_4^- and/or DMSO ligands, analyses of the full width at half maximum (FWHM) of the band at $\nu_4 = 628\,\mathrm{cm}^{-1}$, associated with $\delta_d(OClO)F_2$ mode, and of bands at 314 and 911 cm^{-1} associated with δ(CSC) and $\rho(CH_3)$ modes, respectively, as a function of temperature were performed (figure 3). FWHM values of the bands at 314, 628, and 911 cm^{-1} are almost constant when the sample is heated to T_{C3}^{h} and then suddenly and sharply increase, which suggests that the phase transition, stable phase Cr 1 → stable phase Rot 2 is related to a dynamical orientational order–disorder process of both

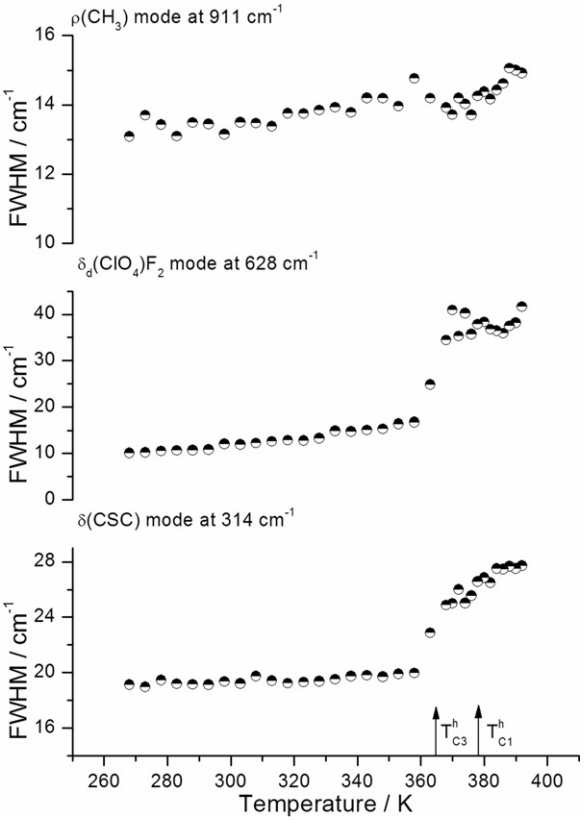

Figure 3. Temperature dependency of the FWHM of the Raman bands associated with δ(CSC), $\delta_d(OClO)F_2$, and $\rho(CH_3)$ modes at 314, 628, and 911 cm^{-1}, respectively. Arrows denote temperature of the phase transitions recorded for $[Mn(DMSO)_6](ClO_4)_2$ by DSC [1] at heating.

DMSO ligands and ClO_4^-. During further heating of the sample, relatively small changes in FWHM values were also detected in the $T_{C1}^h \approx 379\,K$ temperature connected with the phase transition, stable phase Rot 2 → stable phase Rot 1 (see figure 3 and compare with figure 1).

Thermal evolutions of the FT-RS spectra recorded during the cooling and subsequent heating of the sample from 272–392 K are presented in figure 4(a) and (b). On cooling of the sample, peculiar increasing of band intensity of the band associated with ν_s(MnO) at *ca* 396 cm^{-1} can be distinctly seen (figure 4a). Below the phase transition at $T_{C4}^c \approx 322\,K$ splitting of the bands at *ca* 347 and 1015 cm^{-1} can be observed (figure 4a), suggesting that at the vicinity of the phase transition at T_{C4}^c, the crystal symmetry is reduced. As can be seen in thermal evolution of spectra recorded during subsequent

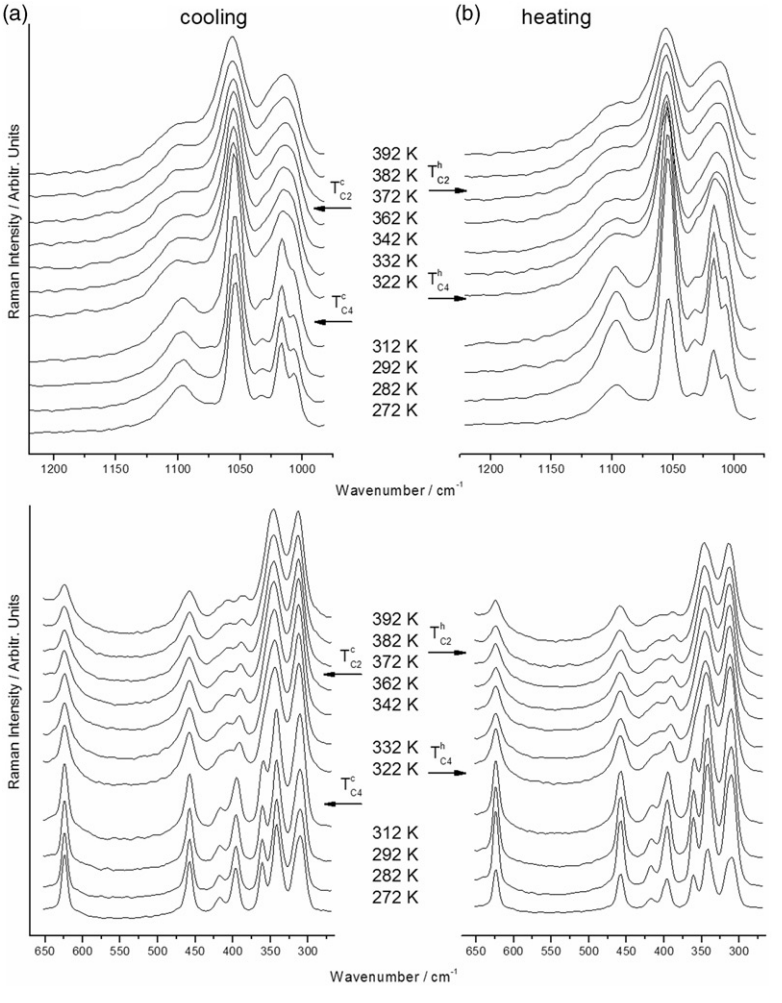

Figure 4. Temperature evolution of the FT-RS spectra recorded at cooling and heating $[Mn(DMSO)_6](ClO_4)_2$. Arrows denote temperature of the phase transitions detected by DSC [1] during cooling T_C^c and heating T_C^h of the sample.

heating of the sample (figure 4b), the phase transition occurring at T^h_{C4} is reversible, therefore above the phase transition temperature at T^h_{C4}, decrease of intensity of the band at *ca* 396 cm^{-1} and reduction of the number of bands in the vicinity of 347 and 1015 cm^{-1} (figure 4b) were again observed.

Figure 5(a) and (b) shows the temperature dependences of FWHM of the bands at 314, 628, and 911 cm^{-1} appointed from spectra recorded during cooling (figure 5a) and subsequent heating (figure 5b) of $[Mn(DMSO)_6](ClO_4)_2$. Analysis of FWHM values as a function of temperature lead to the conclusion that the phase transitions: supercooled phase Rot 1 ↔ metastable phase Rot 3, and metastable phase Rot 3 ↔ metastable phase Cr 3, at $T^c_{C2} \approx 376$ K and $T^c_{C4} \approx 322$ K, respectively, are associated with very small change of reorientational dynamics of the DMSO ligands and ClO_4^- ions. It can also be concluded that these two-phase transitions are reversible (compare with the diagram in figure 1). These two different temperature dependences of FWHM (compare figure 3 with figure 5b) are fully consistent with the phase polymorphism presented as G *versus T* diagram in figure 1.

3.2. *^{1}H NMR measurements*

The second moment and the slope line width of ^{1}H NMR line are usually used to characterize the absorption in radio frequency field [22, 23]. In the shape of the ^{1}H NMR line recorded at first heating (I) from RT, one may distinguish two components,

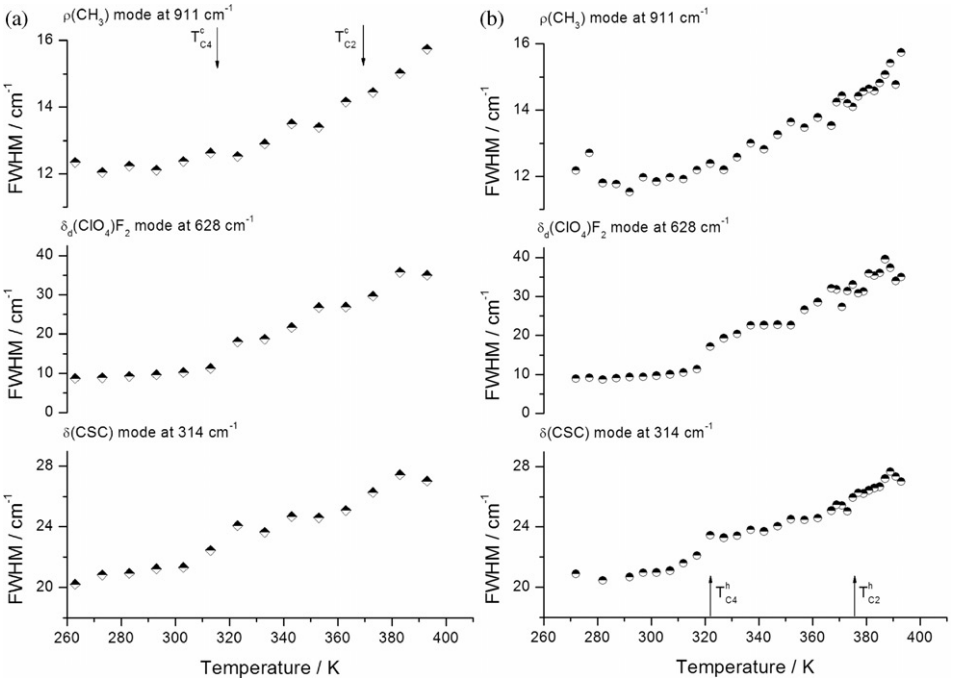

Figure 5. Temperature dependency of the Raman band FWHM associated with δ(CSC), δ_d(OClO)F_2, and $\rho(CH_3)$ modes at 314, 628, and 911 cm^{-1} during (a) cooling and (b) heating of $[Mn(DMSO)_6](ClO_4)_2$. Arrows denote temperature of the phase transition observed by DSC [1].

the broad and the narrow ones. The ratio of the area under both components is 1 : 3. Figure 6(a) shows the influence of temperature on the slope line width (δ_H). On first heating from 300 to 370 K it takes values of 9.5×10^{-4} T and 3.3×10^{-4} T, while from 376–390 K they are 8.0×10^{-4} T and 0.6×10^{-4} T, respectively. Figure 6(b) shows the temperature dependence of the second moment M_2 of ^{1}H NMR line for the compound under study. On first heating the value of the second moment M_2 changes from $(21 \pm 2) \times 10^{-8}$ T^2 at 290 K to $(14.6 \pm 1.5) \times 10^{-8}$ T^2 at 390 K. On the second heating M_2 decreases from $(42 \pm 2) \times 10^{-8}$ T^2 at 100 K to $(32.5 \pm 2) \times 10^{-8}$ T^2 at 200 K and above 225 K it takes the value of $(1 \pm 1) \times 10^{-8}$ T^2.

In order to propose a model of internal dynamics, the second moment of the ^{1}H NMR line was calculated in terms of the dipole–dipole BPP theory, from the van Vleck formula:

$$M_2 = \frac{3}{5}\gamma^2\hbar^2 I(I+1)\frac{1}{N}\sum_{j\neq k}^{N}\frac{1}{r_{jk}^6} \tag{1}$$

where γ = magnetogyric ratio of hydrogen, spin $I = ½$, N = number of protons in elementary unit and r_{jk} = inter-proton distance [24]. Taking into account the crystal structure [17], the bond lengths of the nearly globular cation $[Mn(OS(CH_3)_2)_6]^{2+}$ (S_6 point group) were Mn–O: 2.157, 2.181, and 2.169 Å, for O–S: 1.501, 1.521, and 1.499 Å, for S–C: 1.723, 1.746, 1.740, 1.773, 1.779, and 1.793 Å and for C–H: 0.96 Å.

The internal motion of nuclei influences the second moment through averaging the local field, which is a product of dipole–dipole interaction. The final value of decreased second moment depends on the geometry of motion as well as single crystal studies on the orientation of the sample *versus* magnetic field. It is known that $M_2 = M_2(\text{intra}) + M_2(\text{inter})$. The intra- and intermolecular contributions to the second moment of the ^{1}H NMR line were calculated for the "rigid structure" [25] as 48.2×10^{-8} T^2 and 0.7×10^{-8} T^2, respectively. The calculated total value of the second moment of ^{1}H NMR line was 48.9×10^{-8} T^2 and is higher than observed at 100 K $(42 \pm 2) \times 10^{-8}$ T^2. These differences between calculated and experimental value of M_2 may be connected with

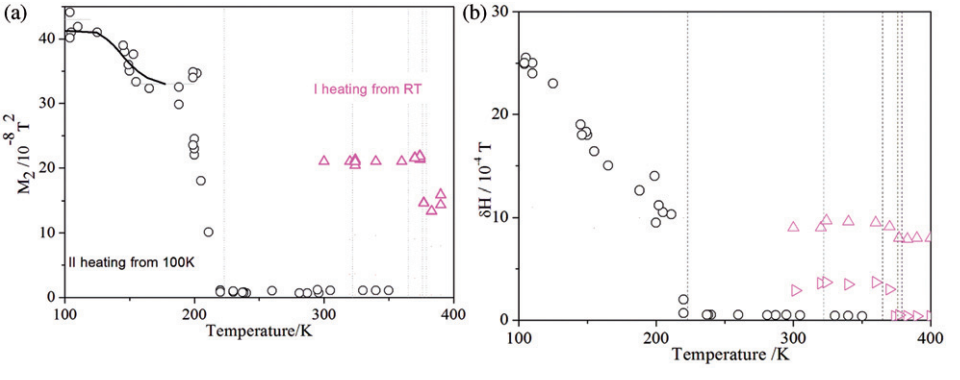

Figure 6. (a) Temperature dependence of the maximum slope line width (δ_H) on first heating of $[Mn(DMSO)_6](ClO_4)_2$ from RT (points: triangles) and on the second heating from 100 K (points: open circles). (b) Temperature dependence of the second moment M_2 of the ^{1}H NMR line of $[Mn(DMSO)_6](ClO_4)_2$.

geometry of the methyl group; it seems that C–H distance is longer than 0.96, as given from the X-ray studies [17, 26].

Reduction in the second moment of the ^{1}H NMR line is observed when the proton–proton vector performs reorientations with a correlation frequency $\nu_c = 1/\tau_c$ on the order of the ^{1}H NMR line width $\sim\delta_H$ (in frequency units) [23, 24, 27]. In our case, τ_c should be in the order of 10^{-3} s. The following internal motions were taken into consideration: (a) reorientations of the methyl group about the C_3 axis; (b) reorientation of the O–S(CH_3) group around the O–S bond; (c) anisotropic reorientation of complex cation around the four-fold symmetry axis; and (d) isotropic reorientation of the whole complex cation.

The decrease in the second moment from $42 \times 10^{-8}\,T^2$ (''rigid lattice'') to $32.5 \times 10^{-8}\,T^2$ corresponds to the four methyl group reorientations about the three-fold symmetry axis around the C–S bond. These methyls belong to the two DMSO ligands of the Mn^{2+}. The jump of DMSO around O–S bond reduces M_2 to $34 \times 10^{-8}\,T^2$. For all methyl group reorientation around the C_3 axis, M_2 decreases to $13.02 \times 10^{-8}\,T^2$. When the isotropic reorientation takes place, the intramolecular contribution to M_2(intra) is reduced to zero and the observed value may be explained only as a result of interactions between the centres of gravity of the complex cation [27].

The area under the ^{1}H NMR absorption signal is proportional to the number of protons. Therefore, at RT the narrow component ($\delta_H = 3.5 \cdot 10^{-4}$ T) of the ^{1}H NMR spectra may be interpreted due to anisotropic reorientation of the complex cation around the four-fold symmetry axis (1/3 of protons participate in this ''slow'' motion), while the other protons participate only in methyl group reorientation (''fast'' motion). Above 376 K, the second moment M_2 of the ^{1}H NMR line decreases from $21 \times 10^{-8}\,T^2$ to $14.6 \times 10^{-8}\,T^2$ and the narrow component of the NMR line is $\delta_H = 0.5 \times 10^{-4}$ T. Analyzing now, the ratio of area under narrow and broad components one may conclude that 1/3 of protons perform isotropic reorientation. Table 2 shows the calculated values of the second moment of ^{1}H NMR line for different motional mechanisms. The calculations of M_2 were performed according to the X-ray data [17]. In many compounds, the C–H distance in methyl is longer than 0.96 Å, up to 1.09 Å [26]. Assuming for methyl, i.e., C–H distance as 0.99 Å and C–C–H angle as 109°, one may obtain the intramolecular value of M_2(intra) as $40.1 \times 10^{-8}\,T^2$. Therefore, observed difference between the low temperature value of M_2 and calculated ones for the rigid

Table 2. Motional parameters of $[Mn(DMSO)_6](ClO_4)_2$ obtained by ^{1}H NMR.

Motion	M_2(intra) + M_2(inter) calculated/$10^{-8}\,T^2$		M_2 experimental/ $10^{-8}\,T^2$	E_a (kJ^{-1} mol^{-1})
Rigid structure	48.2	0.7	42 ± 2	
C_3 reorientation of CH_3 of 4CH_3 groups from 2DMSO ligands	36.0	0.6	32 ± 2	12
C_3 reorientation of methyl around C–S bond accompanied by jump around S–O bond of 2 DMSO	34.0	0.6	32 ± 2	
All methyl C_3 reorientation and the anisotropic reorientation of 1/3 DMSO	19.0	0.6	22 ± 2	
C_3 reorientation of all (12) CH_3 groups	13.3	0.5	15 ± 1	
All methyl C_3 reorientation and the isotropic reorientation of 1/3 molecules	9.3	0.5	15 ± 1	
Isotropic reorientation of the cation	0.0	1.0	1 ± 1	

structure suggests that the position of protons determined by X-ray diffraction is with a margin of error, because of low density of the electron cloud of hydrogen.

From the temperature dependence of the second moment, when it decreased continuously, motional parameters like correlation time and activation energy can be determined using the expression [28, 29]:

$$M_2 = M_{2REO} + (M_{2RIGID} - M_{2REO})\frac{2}{\pi}\mathrm{arctg}\left(\alpha\gamma\sqrt{M_2}\tau_c\right) \quad (2)$$

where M_2 = second moment at temperature T, α = parameter close to 1 and M_{2REO} and M_{2RIGID} = the second moments obtained when Arrhenius correlation time τ_c of molecular group reorientation takes the value $\tau_c^{-1} \gg (M_2)^{1/2}$ or $\tau_c^{-1} \ll (M_2)^{1/2}$, respectively. The activation energy of four methyl reorientation is close to $12\,kJ \cdot mol^{-1}$. The process of isotropic reorientation of cation occurs, while temperature increases from 100 K at the phase transition temperature of 232 K. When heating starts at RT above 376 K, the orientational disorder appears as tumbling process of 1/3 protons per one cation.

4. Conclusions

The characteristic changes of the FT-RS spectra of $[Mn(DMSO)_6](ClO_4)_2$ at the phase transitions temperatures T_{C4} and T_{C3}, connected with both the shift of band positions and the scattered light intensity changes of the bands associated with ν_s(SO), ν_s(MnO), δ(CSC), and δ(OMnO) modes, suggest that these phase transitions are associated with the crystal structure changes. The temperature dependences of these modes indicate crossover behavior between the displacement and order-disorder type of the observed phase transition.

From the temperature dependences of FWHM of the bands associated with the δ(CSC), $\rho(CH_3)$, and $\delta_d(OClO)F_2$ modes in the Raman spectra, we can conclude that the reorientation motions of DMSO ligands and ClO_4^- significantly contribute to the high temperature phase transitions mechanism.

By ^{1}H NMR studies, the following properties of $[Mn(DMSO)_6](ClO_4)_2$ in the solid phases were observed: (1) on heating from RT to 370 K, 1/3 of complex cations perform anisotropic reorientation, while above 376 K they undergo isotropic reorientation. Moreover, fast methyl group reorientation of residue cations has influence on the internal dynamics; (2) after cooling a sample being in plastic phase Rot. 1 from 390 to 100 K and again heating from 100 to 400 K, reorientations of the subsequent methyls about the C_3 axis and finally an isotropic reorientation of the whole cation occur; and (3) ^{1}H NMR studies reveal the reorientational dynamics involved in different phases and give activation parameters of the four methyls (from among the 12 groups in the isolated cation) reorientation with frequencies of a few kHz.

Acknowledgments

Our thanks are due to Professor Edward Mikuli from the Faculty of Chemistry of the Jagiellonian University for stimulating discussions.

References

[1] A. Migdał-Mikuli, E. Szostak. *Z. Naturforsch. A*, **60**, 289 (2005).
[2] E. Szostak, A. Migdał-Mikuli, E. Szostak, A. Kaczor, W. Nitek. *Spectrochim. Acta A*, **79**, 1179 (2011).
[3] A. Migdał-Mikuli, E. Mikuli, E. Szostak, J. Serwońska. *Z. Naturforsch. A*, **58**, 341 (2003).
[4] A. Migdał-Mikuli, E. Szostak. *Thermochim. Acta*, **426**, 91 (2005).
[5] G.J. Kabo, A.A. Kozyro, V.V. Diky, V.V. Simirsky, L.S. Ivashkevich, A.P. Krasulin, V.M. Sevruk, A.P. Marchand, M. Frenkel. *J. Chem. Thermodyn.*, **27**, 707 (1995).
[6] M.B. Charapennikau, A.V. Blokhin, G.J. Kabo, A.G. Kabo, V.V. Diky, A.G. Gusakov. *Thermochim. Acta*, **382**, 109 (2002).
[7] J.M. Pringle, J. Adebahr, D.R. MacFarlane, M. Forsyth. *Phys. Chem. Chem. Phys.*, **12**, 7237 (2010).
[8] J.N. Sherwood. *Plastically Crystalline State; Orientationally Disordered Crystals*, John Wiley & Sons Ltd, London (1979).
[9] Y. Abu-Lebdeh, P.J. Alarco, M. Armand. *J. New Mat. Electrochem. Syst.*, **7**, 29 (2004).
[10] T. Luty, K. Rohleder, J. Lefebvre, M. Descamps. *Phys. Rev. B*, **62**, 8835 (2000).
[11] H. Suga, S. Seki. *J. Non-Cryst. Solids*, **16**, 171 (1974).
[12] A. Abouimrane, P.S. Whitfield, S. Niketic, I.J. Davidson. *J. Power Sources*, **174**, 883 (2007).
[13] M. Patel, K.G. Chandrappa, A.J. Bhattacharyya. *Electrochim. Acta*, **54**, 209 (2008).
[14] Y. Abu-Lebdeh, A. Abouimrane, P.J. Alarco, M. Armand. *J. Power Sources*, **154**, 255 (2006).
[15] Y. Abu-Lebdeh, A. Abouimrane, P.J. Alarco, I. Dividson, M. Armand. *J. Power Sources*, **159**, 891 (2006).
[16] P.J. Alarco, Y. Abu-Lebdeh, A. Abouimrane, M. Armand. *Nat. Mater.*, **3**, 476 (2004).
[17] A. Migdał-Mikuli, E. Szostak, W. Nitek. *Acta Cryst. E*, **62**, m2581 (2006).
[18] Raman/IR Atlas, Verlag Chemie GmbH, Weinheim, Bergstr. (1974).
[19] K. Nakamoto. *Infrared and Raman Spectra of Inorganic and Coordination Compounds*, 6th Edn, p. 107, Part B, John Wiley & Sons, New York (2009).
[20] E. Szostak, K. Drużbicki, E. Mikuli. *J. Mol. Struct.*, **970**, 139 (2010).
[21] C.V. Berney, J.H. Weber. *Inorg. Chem.*, **7**, 283 (1968).
[22] E.R. Andrew. *Nuclear Magnetic Resonance*, University Press, Cambridge, UK (1956).
[23] C.P. Slichter. *Principles in Magnetic Resonance*, Springer Verlag, Berlin, Heidelberg, New York (1978).
[24] J.H. van Vleck. *Phys. Rev.*, **74**, 1168 (1948).
[25] C.F. Macrae, J.A. Bruno, J.A. Chisholm, P.R. Edgington, P. McCabe, E. Pidcock, L. Rodriguez-Monge, R. Taylor, J. van de Streek, P.A. Wood. *J. Appl. Cryst.*, **41**, 466 (2008); C.F. Macrae, P.R. Edgington, P. McCabe, E. Pidcock, G.P. Shields, R. Taylor, M. Towler, J. van de Streek. *J. Appl. Cryst.*, **39**, 453 (2006); I.J. Bruno, J.C. Cole, P.R. Edgington, M.K. Kessler, C.F. Macrae, P. McCabe, J. Pearson, R. Taylor. *Acta Cryst. B*, **58**, 389 (2002); R. Taylor, C.F. Macrae. *Acta Cryst. B*, **57**, 815 (2001); F.H. Allen. *Acta Cryst. B*, **58**, 380 (2002).
[26] E.R. Andrew, R.G. Eades. *Proc. Royal Soc. A*, **216**, 537 (1953).
[27] G.W. Smith. *J. Chem. Phys.*, **42**, 4229 (1965).
[28] H.S. Gutowsky, G.E. Pake. *J. Chem. Phys.*, **18**, 162 (1950).
[29] R. Kubo, K. Tomita. *J. Phys. Soc. Jpn.*, **9**, 888 (1954).